Development of whole-body representation and dose calculation in a commercial treatment planning system

Pascal Hauri[1,2,4], **Stephan Radonic**[1,2,*,4], **Fabiano Vasi**[1,2], **Marina Ernst**[1], **Marcin Sumila**[1,2], **Matthew M. Mille**[3], **Choonsik Lee**[3], **Matthias Hartmann**[1,2], **Uwe Schneider**[1,2]

[1] Department of Physics, University of Zurich, Zurich, Switzerland
[2] Radiotherapy Hirslanden, Hirslanden Medical Center, Aarau, Switzerland
[3] Division of Cancer Epidemiology and Genetics, National Cancer Institute, National Institutes of Health, Rockville, MD 20850, USA

Abstract

For the epidemiological evaluation of long-term side effects of radiotherapy patients, it is important to know the doses to organs and tissues everywhere in the patient. Computed tomography (CT) images of the patients which contain the anatomical information are sometimes available for each treated patient. However, the available CT scans usually cover only the treated volume of the patient including the target and surrounding anatomy. To overcome this limitation, in this work we describe the development of a software tool using the Varian Eclipse Scripting API for extending a partial-body CT to a whole-body representation in the treatment planning system for dose calculation. The whole-body representation is created by fusing the partial-body CT with a similarly sized whole-body computational phantom selected from a library containing 64 phantoms of different heights, weights, and genders. The out-of-field dose is calculated with analytical models from the literature and merged with the treatment planning system-calculated dose. To test the method, the out-of-field dose distributions on the computational phantoms were compared to dose calculations on whole-body patient CTs. The mean doses, D2% and D98% were compared in 26 organs and tissues for 14 different treatment plans in 5 patients using 3D-CRT, IMRT, VMAT, coplanar and non-coplanar techniques. From these comparisons we found that mean relative differences between organ doses ranged from −10% and +20% with standard deviations of up to 40%. The developed method will help epidemiologists and researchers estimate organ doses outside the treated volume when only limited treatment planning CT information is available.

Keywords: Whole-body dose, Phantoms, TPS

1 Introduction

In developed countries, more than half of all cancer patients receive radiotherapy at some stage in the management of their disease. Advances in cancer treatment have steadily improved survival times over the past four decades and the number of cancer survivors continues to increase reflecting advances in early detection and treatment as well as the overall aging and growing population. In 1971, three million people were living with cancer in the US population. In 2016, already more than 15.5 million Americans with a history of cancer were alive and this number is projected to reach more than 20 million by 2026 [1,2]. In the absence of other competing causes of death, 64% of adults whose cancer was diagnosed during 1995 and 2000 could expect to be alive 5 years after diagnosis, compared with 50% for those whose cancer was diagnosed during 1974

---

and 1976. Among children, the improvement of cure rates is even more pronounced with 83% five-year cancer survivors (2005–2010), compared with 58% after diagnosis during 1975 and 1977 [1].

Among all cancer survivors in 2016, 21% of female survivors were diagnosed more than twenty years ago compared to 13% of males [1]. Approximately half of these long-term survivors received a radiotherapy treatment and are thus subject to radiation-related side effects. These long-term survivors experience a significant incidence of chronic health problems after their treatment, including second primary cancer [2]. A second cancer is defined as a histologically distinct cancer that develops after the first cancer. In total, 95,000 of the 1.2 million new cancers diagnosed every year in the United States are second cancers [3]. Second cancers therefore account for 6–10% of all cancer diagnoses. A radiation-induced secondary malignancy can be the price of success, if the primary cancer is cured or at least controlled. Radiation Therapy increases the risk of second cancer by 1.2-fold to 3-fold in adults and by 6-fold to 10-fold in pediatric patients.

Research and development in radiation oncology is mainly directed to further increase cure rates. This is currently achieved by the application of new radiation treatment modalities such as intensity-modulated radiotherapy (IMRT), volumetric-modulated arc therapy (VMAT), proton and heavy ion radiotherapy. These newer treatment modalities better localize the high radiation dose to the target, but sometimes at the expense of exposing a larger volume of the body to a low radiation dose [4]. As dose is a major risk factor for the development of second malignancies [5,6], it will take decades of follow-up to fully understand how these new treatments impact the long-term health of cancer survivors.

The major input for radiation risk models is the three-dimensional (3D) distribution of dose within the patient. While the dose calculations in the surrounding tissues of the target are precise (on order of a few %), several research groups have sought to develop analytical dose algorithms as well as Monte Carlo methods to improve dose estimates in the out-of-field region [7–10].

However, a major problem in calculating the whole-body dose and finally second tumor risk in radiotherapy is that the treatment planning is typically performed using a partial-body CT. To minimize the radiation exposure, the scan range typically covers only the area of interest to the treatment, whereas second tumors can sometimes occur outside the scanned region [11]. Therefore, alternative approaches are necessary to allow a whole-body dose calculation. At least the surface and critical structures of the patient are needed for out-of-field dose computations. Whole-Body computational human phantoms can be used to provide extended anatomy of out-of-scan organs [12–14]. By fusing the partial-body CT of the patient with a computational human phantom, a whole-body representation of the patient can be created.

Kuzmin et al. [12] reported a novel method to extend a partial-body CT to a whole-body CT for the purpose of the calculation of out-of-field organ doses for patients who underwent external radiotherapy. They selected a computational human phantom by matching a given patient's height and weight from a library of 351 pediatric and adult computational human phantoms covering different body sizes [15]. A whole-body anatomy was created by combining the original RT Image and RT Structure files of a patient with the selected phantom. The authors confirmed that their method results in improved dosimetric accuracy for external radiotherapy patients compared to the results only based on whole-body phantoms after applying their method for chest and prostate irradiation cases [12].

Models for calculating the out-of-field dose have been historically available for the purpose of dose calculations for epidemiological studies for RT patients [16]. These models either lack the generalization to more advanced treatment techniques such as IMRT [10] or do not model all relevant scatter radiation. The novelty of this work is the creation of a patient-specific whole-body representation which is embedded in a commercial TPS. In comparison to the work of Kuzmin et al. [12], the implemented dose calculation engine calculates all radiation scatter contributions separately, including neutron dose and is applicable to complex photon radiotherapy techniques such as IMRT or VMAT.

The authors are of the opinion that with this work a truly patient-specific whole-body dose estimation in photon radiotherapy is achieved.

2 Materials and method

2.1 Whole-body representation

A software solution was developed which automatically fuses a partial-body CT with a whole-body computational human phantom. The phantom is selected from a sophisticated library of computational phantoms by using the patient's size and weight [15]. For the current work, the whole-body phantom library contained 64 phantoms of both genders (male and female) and various heights and weights to cover typical sizes of radiotherapy patients. The heights of the phantoms ranged from 50 to 190 cm with weights of 5 to 130 kg. The phantoms were derived from a pre-existing library of 351 pediatric and adult phantoms [15], which was extended from ten pediatric and two adult male and female reference size phantoms developed in the collaboration between the University of Florida and the National Cancer Institute [17]. The reference phantoms were developed from patient CT images in the format of Non-Uniform Rational B-Spline (NURBS), which was non-uniformly transformed to match the reference organ mass [18], gastrointestinal tract mass and dimension [19], and standard elemental composition and density [20]. The 64 adult male and female phantoms were converted to DICOM CT format with an accompanying DICOM-RT structure set (RTSTRUCT) containing the organ contours for the whole-body phantom [21].
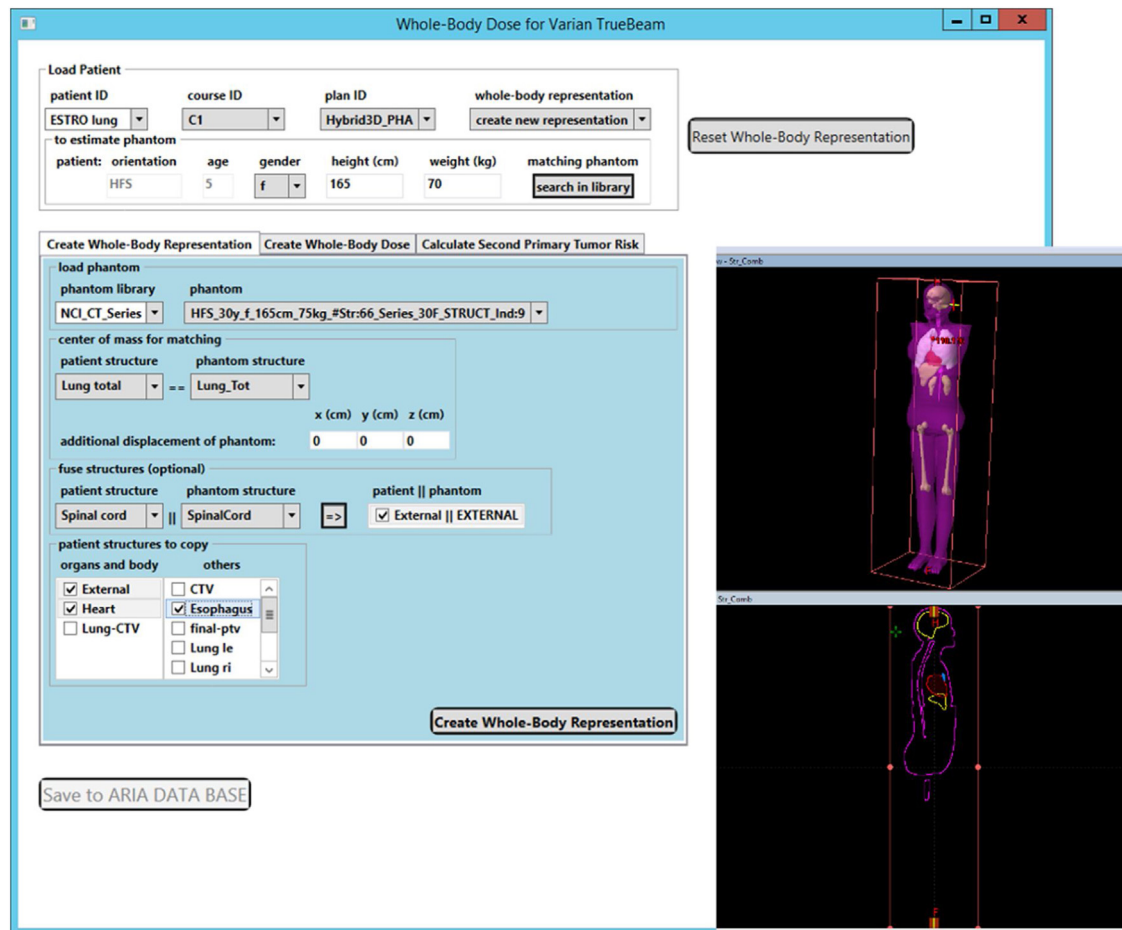
Figure 1. The user interface for the creation of the whole-body representation. On the right side the whole-body representation of a lung patient is shown in the Eclipse TPS.

The following paragraph describes how the software uses scripting application programming interface (API) within the Eclipse treatment planning system (TPS) (Varian Medical Systems, Palo Alto, CA, USA) to generate the patient's whole-body representation and dose distribution.

To create a patient-specific whole-body representation, a rigid registration algorithm is used to merge the patient and phantom body structures (organ delineation sets). To this end, a structure which is completely included in the limited CT as well as in the virtual NCI phantom, is chosen by the user. The center of mass of this structure is then used to align the patient image with the phantom image. Structures which are partly contained in the original CT can be merged with the corresponding structure in the phantom. The final structure consists then of the original structure in the volume of the original CT and of the phantom structure outside the CT. In this way the original patient structures are consistently extended. By pressing the button "Create Whole-body Representation",

the desired phantom-patient hybrid structure set is created. From here on the term "phantom" is interchangeably used with the term "whole-body representation". A progress report window shows the different actions taken by the program during creation. In the whole-body representation the density of air is automatically assigned to all lung structures while the density of water is assigned to all other structures including the body. After successfully generating the representation, the user can optionally save the result to the TPS database or can proceed directly to the next step. Saving the result allows the user to view the whole-body representation in Eclipse TPS.

Figure 1 shows the user interface of the program. The user selects a patient and the treatment plan for which the whole-body representation should be constructed. The partial-body CT is merged with a whole-body phantom selected from a library. Any library of phantoms can be used provided that the DICOM-RT structure sets (RTSTRUCT) are existing in the TPS.
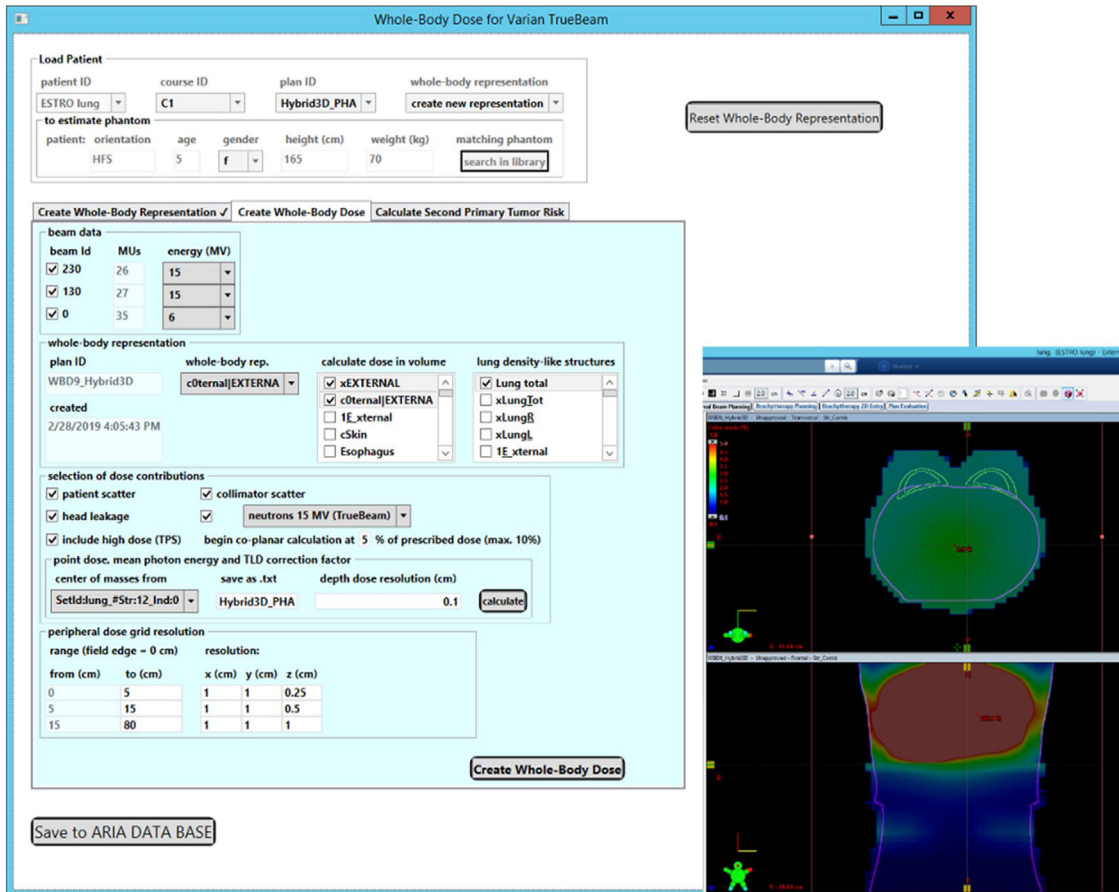
Figure 2. The tab of the whole-body dose creation. After completing this step and saving to the database the whole-body dose can be calculated and viewed in Eclipse (as shown on the right). A continuous translation between the TPS and the algorithm-calculated 3D dose distribution can be seen.

2.2 Whole-body dose

Figure 2 shows the section of the program to calculate the dose distribution. The user selects a whole-body representation and a treatment plan for which the whole-body dose shall be calculated on. Hauri et al. [22,7] describe how the peripheral-dose is calculated and subsequently merged with the TPS calculated dose. In summary, phantom scatter, collimator scatter, leakage dose and neutron dose are calculated for a specific Linac and treatment plan. The whole-body dose consists of the original dose calculated by the treatment planning system and the out-of-field dose, both of which are merged at the 5% isodose.

The accuracy of the whole-body dose calculation was previously evaluated by comparing calculations to experimental measurements. For twelve treatments of different indications (Hodgkin disease, ependymoma in the head, and rhabdomyosarcoma in the prostate), the whole-body dose was measured using a male and female anthropomorphic Alderson phantom. The measurements are explained in detail in a separate publication by Hauri et al. [22]. The dose was delivered by

three different modalities (3D-CRT, IMRT, and VMAT) using two nominal beam energies (6 MV and 15 MV). For each treatment, anthropomorphic Alderson phantoms were loaded with around 400 thermoluminescent dosimeters and the dose was delivered. It was found that in the peripheral dose region, the calculated stray dose agreed within $10 \pm 22\%$ (mean and standard deviation) compared to the measurements. The measured stray dose for the twelve treatments contained the secondary photon and neutron dose [22].

2.3 Verification of the whole-body representation

The correctness of the described method to create a patient-specific whole-body representation was tested by comparing the dose in a patient's whole-body CT and the dose in their respective whole-body representation. Firstly, a registration between the whole-body CT and the phantom was performed using a structure lying in the treated volume. Since the patient CT was not limited, a merging of the CT and phantom was not necessary (e.g., see Figure 3). By calculating the out-of-field dose in the original patient CT and in the phantom, a

Figure 3. The sagittal and coronal views of a 30-year-old female patient with breast cancer; CT overlayed with selected structures (organ delineation sets) of the virtual phantom. Orange – body outline of virtual NCI Phantom, Blue – Brain, Violett – Small Bowel, Purple – Liver, Violett – Colon, Magenta – Esophagus, Green – Heart, Black – Kidneys, Dark Blue – Lungs, Light Green – Stomach, Yellow – Fetus trunk.

one-to-one comparison of the dose in various organs could be performed and quantitatively analyzed.

Figure 3 shows the sagittal and coronal views of a 30-year-old female patient with breast cancer. The images show the CT overlayed with selected structures of the virtual NCI phantom.

Four patients of different sizes were selected for the comparison. For each patient a typical tumor indication was selected and an appropriate target was defined. Treatment plans using different techniques (3D-CRT, IMRT, VMAT) and different nominal beam energies (6 and 15 MV) were designed. Dose was calculated using the Eclipse V15.6 TPS. Afterwards a whole-body representation was created and the out-of-field dose was computed on the original CT as well as on the whole-body representation and merged with the TPS-dose. The TPS dose was used wherever the dose was larger than 5% of the prescribed dose on the cranial-caudal axis of the

whole-body phantom. Everywhere else the out-of-field dose calculation was used. For each organ in the original whole-body CT scan as well as in the whole-body representation (phantom), the differential dose volume histogram (DVH) was exported from the TPS. For each DVH, the mean dose, $D_{98\%}$, and $D_{2\%}$ were calculated, where $D_{98\%}$ and $D_{2\%}$ represent the minimum dose received by 98% and 2% of the organ volume, respectively. The mean dose, $D_{98\%}$, and $D_{2\%}$ in the organs of the whole-body CT scan and the whole-body representation were compared if $D_{2\%}$ was smaller than 5% of the prescribed dose. The 5% level was chosen because we are interested in a verification of out-of-field doses and above this level the dose was calculated by the TPS.

The whole-body CT scans of 4 patients (8-week-old baby, 7-year-old child, 30-year-old pregnant woman, and a 38-year-old man) were downloaded from the web page of the

Helmholtz Zentrum Munich [23]. The DICOM files were imported into the Eclipse TPS and contained all the relevant structures for dose comparison.

In a next step the targets and dose prescriptions for treatment planning were defined. In the 8-week-old baby a target representing a gluteal rhabdomyosarcoma on the right side was drawn. A dose of 31.2 Gy was prescribed in two daily fractions of 1.2 Gy, 5 times a week. The same schedule was used for the 7-year-old child, with the target being an osteosarcoma of the right middle ear. For the 30-year-old pregnant woman a breast target was selected. A radiotherapy schedule after breast conserving surgery of nodal positive right-sided breast cancer was used. The target included the whole right breast and the ipsilateral supraclavicular and internal mammary lymph nodes stations with a total of 50 Gy delivered in 25 fractions (2 Gy per fraction). For the 38-year-old male two targets were defined. The first one was a mediastinal Hodgkin disease with a dose of 30 Gy delivered in 15 fractions (2 Gy per fraction). The second one was a typical seminoma target for which a paraaortic radiotherapy with 20 Gy delivered in 10 fractions (2 Gy per fraction).

Several different treatment plans were created within the Eclipse V15.6 TPS for each one of the five tumors. The treatment plans represent various potential and feasible irradiation techniques with either one of the two photon energies 6 MV or 15 MV, to irradiate these patients. For the 8-week-old baby with the gluteal target only 6 MV photon beams were used. Three plans were realized. One plan was a 3D conformal plan with three coplanar fields with dynamic wedges. The second plan contains seven coplanar IMRT fields. In addition, a VMAT plan was created using 2 coplanar arcs, each with an avoidance angle of 120 degrees over the contralateral side. The matching of the patient CT with the phantom was performed using the liver structure. For the 7-year-old child with the tumor in the middle ear three plans with 6 MV photon beams were created. The first plan is a VMAT plan with two arcs. The second plan was created with eight non-coplanar static IMRT fields. Additionally, a VMAT plan was created with two non-coplanar arcs, both containing avoidance angles of 120 degrees over the contralateral side of the head. The matching of the patient image with the phantom image was performed on the brain. Two therapy plans were prepared for the 30-year-old pregnant woman with a breast tumor. One plan was created with two tangential IMRT fields for the irradiation of the right breast and a third static field with a dynamic wedge for the supraclavicular lymph nodes. In the other plan, the sternal lymph nodes got included as well. The irradiation was planned as a hybrid plan with two tangential IMRT fields and two VMAT fields which cover the supraclavicular and sternal lymph nodes. The match of the patient image with the phantom image was performed on the right lung. The 38-year-old man with the Hodgkin lymphoma got two plans with two opposing static IMRT fields and two plans containing two opposing static fields with dynamic wedges. For either technique, 6 MV photons were used in one plan and

15 MV in the other. The matching of the patient image with the phantom image was performed on the left lung. The 38-year-old male patient with the seminoma was planned with two opposing static 6 MV photon fields and in another plan with two opposing static 15 MV photon fields. The matching of the patient image with the phantom image was performed on the liver.

In Table 1, an overview of the target, dose prescription and treatment plans for each patient is listed.

3 Results

In the following sections we are presenting the comparisons for the different patients. Detailed results are only shown for the 30-year-old female with breast cancer. For the other patients only summarized results are shown. Details can be found in the supplementary material.

3.1 30-year-old female with breast cancer

The 30-year-old female with breast cancer was matched to a 30-year-old female phantom with a height of 165 cm and weight of 60 kg. Figures 4 and 5 show the dose differences between the dose calculation performed on the original CT and the phantom for IMRT/3D-CRT and IMRT/VMAT plan, respectively. The average differences between the mean dose in 19 out-of-field organs including the fetus for the mixed IMRT/3D-CRT plan were 4.7 mGy and the standard deviation was found to be 56.9 mGy. The maximum deviation of the mean dose in the phantom compared to the original patient is −89.8% and is found in the mandible. The best match for the mean doses in the original patient and the phantom was in this plan found for the heart with a deviation of −0.3%. For the combined IMRT/VMAT plan the average difference of the mean dose was 11 mGy with a standard deviation of 59 mGy. The maximum deviation of the average dose in the phantom compared to the original patient is 63.8% and is found in the uterus. The best match for the mean doses in the original and the phantom was in this plan found for the liver with a deviation of 0.4%.

In Figure 6, a histogram of the relative differences of the mean doses in all organs and for all treatment plans is plotted.

When radiotherapy is planned for young women, the question can arise whether a treatment of a pregnant patient is justified. For the decision-making, a good knowledge of the dose to the fetus is required. Therefore, a pregnant patient including a fetus was chosen for this comparison. The mean fetus doses are shown in Figures 4 and 5. In addition the dose volume histograms of the fetus for the IMRT/static and the IMRT/VMAT plans are shown in Figures 7 and 8, respectively. The DVHs look similar for both treatment plans. For the IMRT/3D-CRT plan the mean fetus dose is 69 mGy in the original patient CT and 72 mGy for the matched phantom. For

Table 1
Overview of patient examples, their characteristics and treatment plans.

| Patient Example	Gender	Structure which was used to match CT and whole-body phantom	Prescribed dose/Gy	Number of fractions	Dose per fraction/Gy	Radiotherapy plans
8-week-old baby with gluteal rhabdomyosarcoma on right side	Female	Liver	31.2	26	1.2	(1) 6 MV, 3DCRT (2) 6 MV, IMRT (3) 6 MV, VMAT
7-year-old child with osteosarcoma of the right middle ear	Female	Brain	31.2	26	1.2	(1) 6 MV VMAT (2) 6 MV, IMRT non coplanar (3) 6 MV, VMAT non coplanar
30-year-old adult with right breast cancer including lymph nodes	Female	Right lung	50	25	2	(1) IMRT (6 MV) + 3DCRT (15 MV) (2) IMRT (6 MV) + VMAT (6 MV)
38-year-old adult with mediastinal Hodgkin lymphoma	Male	Left lung	30	15	2	(1) 6 MV, IMRT (2) 15 MV, IMRT (3) 6 MV, 3DCRT (4) 15 MV, 3DCRT
38-year-old adult with seminoma	Male	Liver	20	10	2	(1) 6 MV, 3DCRT (2) 15 MV, 3DCRT
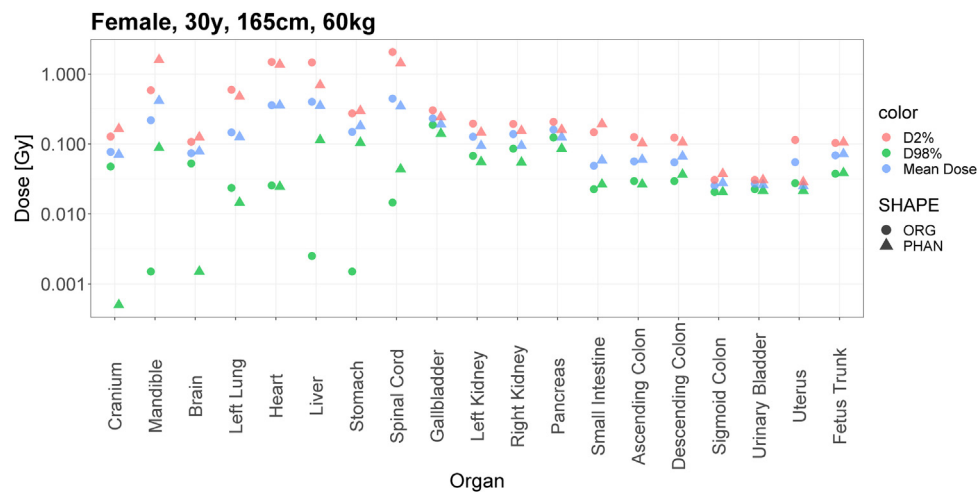
Figure 4. Out-of-field dose comparison between the original patient (circles) and the phantom (triangles) in different organs. The patient is a 30-year-old pregnant woman with a breast tumor. The chosen computational human phantom from the above-mentioned library was female, 30-year-old, 165 cm tall and weight of 60 kg. This RT plan consists of two tangential IMRT fields with a static field for the lymph nodes. The plot shows the values for $D_{2\%}$ (red), the mean dose (blue), and the near minimal dose $D_{98\%}$ (green).

the IMRT/VMAT plan the mean fetus dose is 134 mGy for the original patient CT and 136 mGy for the matched phantom.

3.2 Eight-week-old baby with a gluteal rhabdomyosarcoma

The baby was matched to the NCI phantom of a female newborn with 65 cm height and 5 kg weight.

The average differences between the mean dose in 13 out-of-field organs for the 3D conformal plan were −1.6 mGy with a standard deviation of 3.8 mGy. The maximum deviation of the mean dose in the phantom compared to the original patient is −17.4% and is found in the esophagus. The best match for the mean doses in the original patient and the phantom in this plan was found for the right lung with a deviation of −1.8%. For the IMRT plan the average difference of the mean dose was
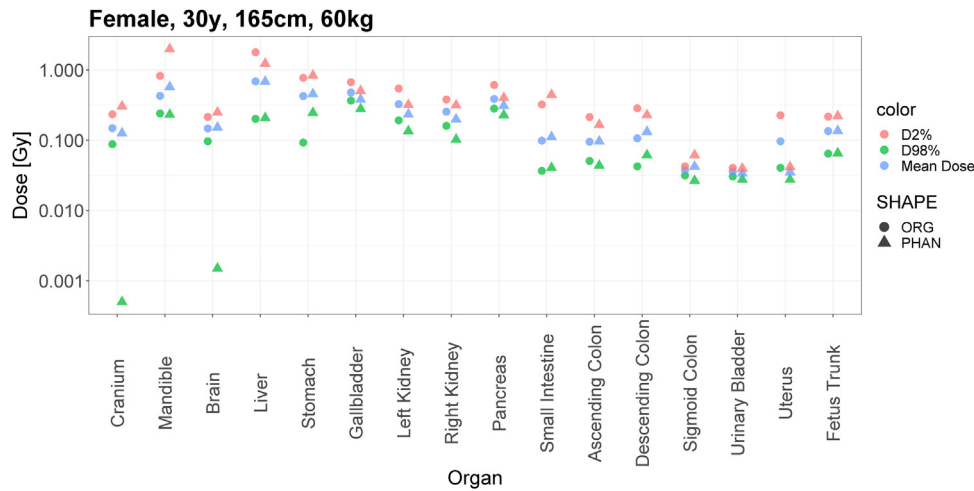
Figure 5. Out-of-field dose comparison between the original patient (circles) and the phantom (triangles) in different organs. The patient is a 30-year-old pregnant woman with a breast tumor. The chosen computational human phantom from the library was female, 30-years-old, 165 cm tall and weight 60 kg. This radiotherapy plan consists of two tangential 6 MV IMRT fields and two 6 MV VMAT fields which cover the supraclavicular and sternal lymph nodes.
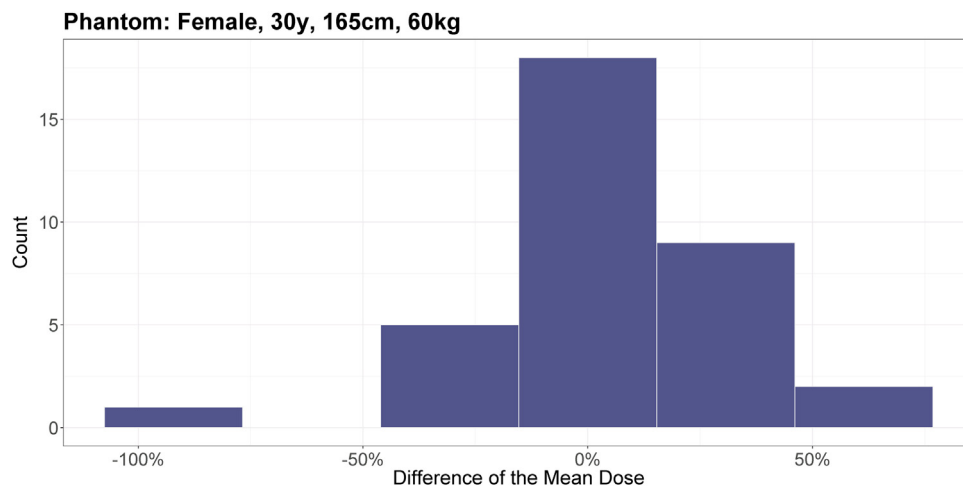

Figure 6. Out-of-field mean dose differences in organs of the original patient compared to the phantom for two radiotherapy plans (see Figures 3 and 4). All organs where $D_{2\%}$ is less or equal to 5% of the prescribed dose are considered. In these two RT plans for the 30-year-old pregnant woman with a breast tumor the difference in the mean dose per organ is 7.5 mGy with a standard deviation of 57.1 mGy. The histogram has a bin width of 0.31.

found to be −9.4 mGy with a standard deviation of 17.8 mGy. The maximum deviation of the mean dose in the phantom compared to the original patient is −25.5% and is found in the right kidney. The best match for the mean doses in the original and the phantom was in this plan found for the right lung with a deviation of −2.5%. Finally, the average difference of the VMAT plan was −9.5 mGy with a standard deviation of 26.3 mGy. The maximum deviation of the mean dose in the phantom compared to the original patient is −109.3% and is found in the right kidney. The best match for the mean doses in the original and the phantom was in this plan found for the heart with a deviation of - 2.6%.

In Figure 9 a histogram of the relative differences of the mean doses in all organs and for all treatment plans is plotted.

3.3 Seven-year-old female child with osteosarcoma of the middle ear

The 7-year-old female was matched to the NCI phantom of a 5-year-old female with 115 cm height and 50 kg weight.

The average differences between the mean doses in 17 out-of-field organs for the IMRT plan were 1.1 mGy with a standard deviation of 18.4 mGy. The maximum deviation of the mean dose in the phantom compared to the original patient
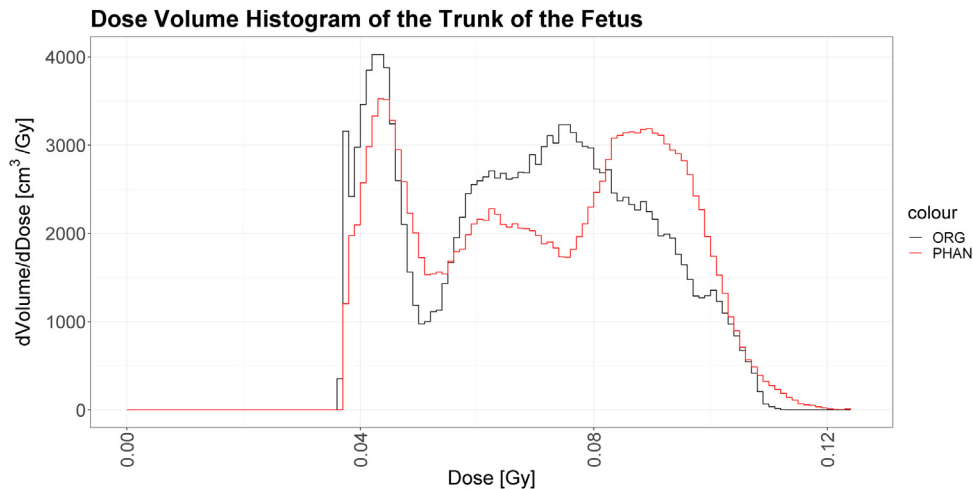
Figure 7. Differential dose volume histogram of the trunk of the fetus. The RT plan consisted of two tangential 6 MV IMRT fields for the irradiation of the right breast and a third static 15 MV field with a dynamic wedge for the supraclavicular lymph nodes. The DVHs from calculated RT plans on the original patient (black) and on the phantom (red) are shown. The mean dose in the fetal trunk from the original plan is 69 mGy. In the case of the phantom, the mean dose in the fetal trunk is 72 mGy.
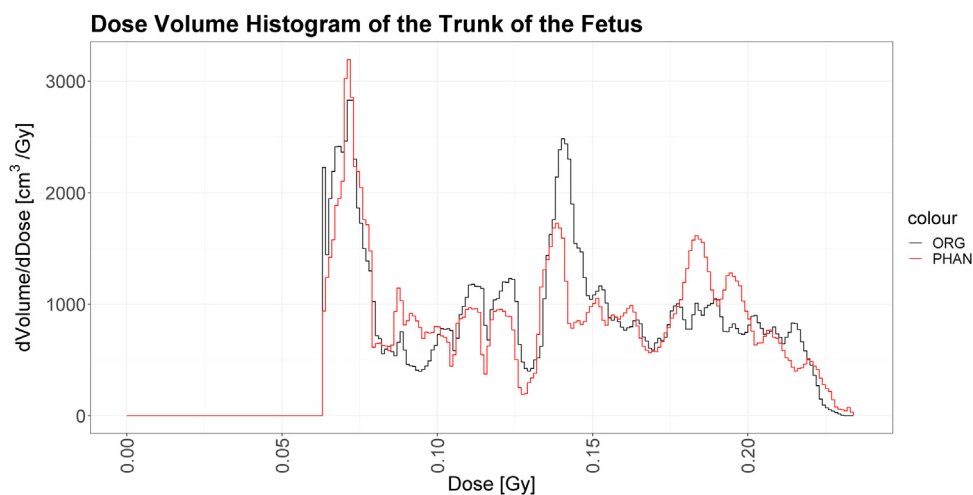

Figure 8. Differential dose volume histogram of the trunk of the fetus. The RT plan consisted of two tangential 6 MV IMRT fields and two 6 MV VMAT fields which cover the supraclavicular and sternal lymph nodes. The DVHs from calculated RT plans on the original patient (black) and on the phantom (red) are shown. The mean dose in the fetal trunk from the original plan is 134 mGy. In the case of the phantom, the mean dose in the fetal trunk is 136 mGy.

was −92.1% and is found in the spinal cord. In this plan there was no deviation found in the mean doses in the foot bones of the original and the phantom. For the coplanar VMAT plan the average difference of the mean dose was found to be 9.4e−02 mGy and the standard deviation was found to be 4.4 mGy. The maximum deviation of the average dose in the phantom compared to the original patient is −59.9% and is found in the spinal cord. The best match for the mean doses in the original patient and the phantom in this plan was found for the bones of the foot where no deviation was found. Finally, the average difference of the non-coplanar VMAT plan was −0.1 mGy with a standard deviation of 5.6 mGy.

The maximum deviation of the average dose in the phantom compared to the original patient is −130% and is found in the spinal cord. Again, no deviation was found in the mean dose of the foot bones of the original and the phantom. In Figure 10 a histogram of the relative differences of the mean doses in all organs and for all treatment plans is plotted.

3.4 Thirty-eight-year-old male with Hodgkin's disease

The 38-year-old male with mediastinal Hodgkin's disease was matched to a 30-year-old male phantom with a height of 175 cm and weight of 65 kg. The average differences between
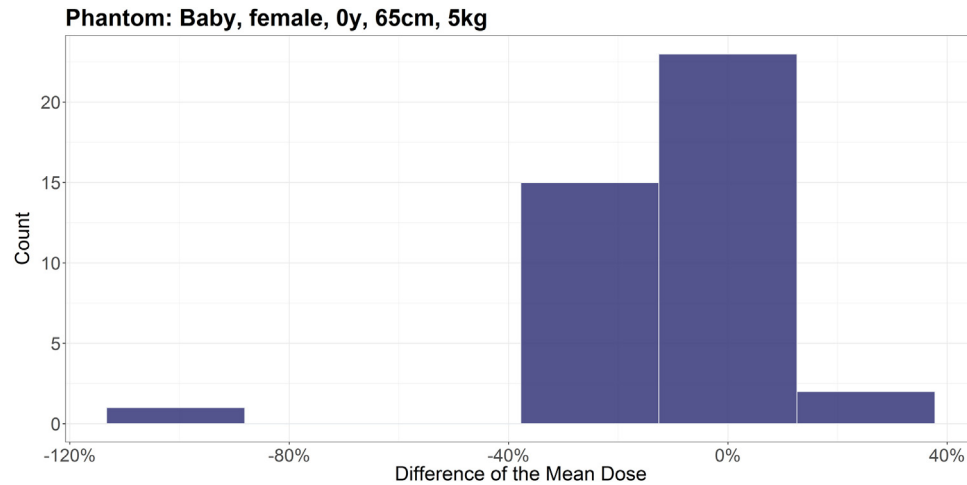
Phantom: Baby, female, 0y, 65cm, 5kg

Figure 9. Out-of-field mean dose differences in the organs of the original whole-body and the phantom in all organs where $D_{2\%}$ is less or equal to 5% of the prescribed dose in the three plans for the 8-week-old baby with a gluteal rhabdomyosarcoma on the right site. In these three plans the mean difference of the mean dose per organ is -7.0 mGy with a standard deviation of 18.6 mGy. The histogram has a bin width of 0.25.
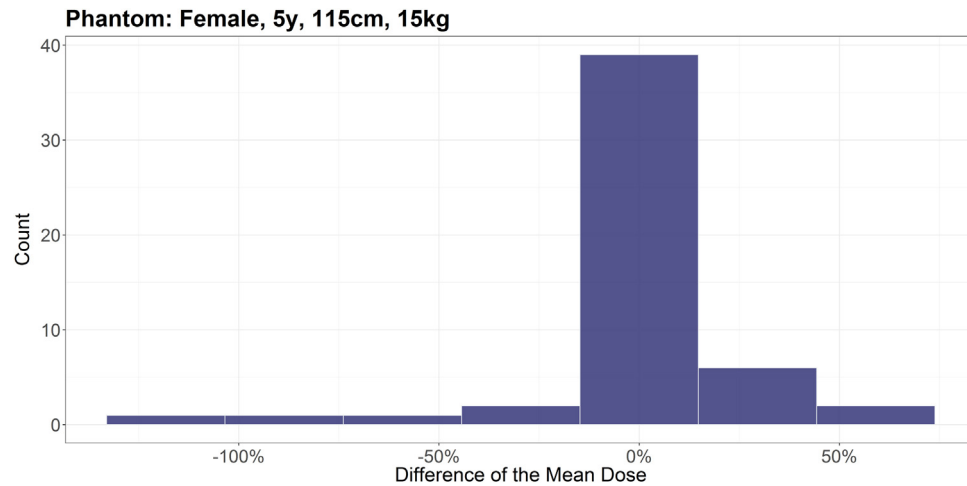
Phantom: Female, 5y, 115cm, 15kg

Figure 10. Out-of-field dose differences between the original whole-body dose representation and the phantom in all organs where the $D_{2\%}$ is less or equal to 5% of the prescribed dose in the three plans for the 7-year-old child with the tumor in the middle ear. In these plans the mean difference of the mean dose per organ is 0.35 mGy with a standard deviation of 11.1 mGy. The histogram has a bin width of 0.30.

the mean dose in 14 out-of-field organs for the 6 MV plan were 114 mGy with a standard deviation of 152 mGy. The maximum deviation of the mean dose in the phantom compared to the original patient is -58.3% and is found in the pancreas. The best match for the mean doses in the original and the phantom was in this plan found for the foot bones where no deviation was found. For the 15 MV plan the average difference of the mean dose was 94.0 mGy with a standard deviation 131.0 mGy. The maximum deviation of the mean dose in the phantom compared to the original patient is 60.2% and is found in the pancreas. The best match for the mean doses in the original and the phantom was in this plan found for the foot bones where no deviation was found.

The treatment was also planned for using static 3D-CRT radiotherapy. The average differences between the mean dose in 14 out-of-field organs for the 6 MV plan were 104.0 mGy with a standard deviation 137.8 mGy. The maximum deviation of the average dose in the phantom compared to the original patient is -60.9% and is found in the pancreas. The best match for the mean doses in the original and the phantom was in this plan found for the foot bones where no deviation was found. For the 15 MV plan the average difference of the mean dose was 71.7 mGy with a standard deviation 98.0 Gy. The maximum deviation of the average dose in the phantom compared to the original patient is 63.4% and is found in the pancreas. The best match for the mean doses in the original and the

Figure 11. Out-of-field dose differences between the original whole-body dose representation and the phantom in all organs where the D2% is less or equal to 5% of the prescribed dose in the four plans for the 38-year-old man with the Hodgkin lymphoma. In these plans the mean difference of the mean dose per organ is 95.8 mGy with a standard deviation of 128.6 mGy. The histogram has a bin width of 0.16.

phantom was in this plan found for the foot bones where no deviation was found.

In Figure 11 a histogram of the relative differences of the mean doses in all organs and for all treatment plans is plotted.

3.5 Thirty-eight-year-old male with Seminoma

The 38-year-old male with a seminoma was matched to the phantom of a 30-year-old male with a height of 175 cm and weight of 80 kg. Although the seminoma target was segmented on the same whole-body CT used for the Hodgkin target, a different phantom was matched to it. The reason for this is that the phantoms were matched to structures in the target regions. The 70 kg phantom used for the Hodgkin patient was fitting better to thoracic region of the CT while the 80 kg phantom fitted better the abdominal region.

The average differences between the mean dose in 11 out-of-field organs for the 3D-CRT plan with 6 MV were −0.34 mGy and the standard deviation was found to be 32.18 mGy. The maximum deviation of the mean dose in the phantom compared to the original patient is −129.7% and is found in the testes. The best match for the mean doses in the original patient and the phantom in this plan was found for the bones of the foot where no deviation was found. The average differences between the mean dose for the 3D-CRT plan with 15 MV were −5.7 mGy with a standard deviation 26.9 mGy. The maximum deviation of the mean dose in the phantom compared to the original patient is −102.2% and is found in the testes. The best match for the mean doses in the original and the phantom was in this plan found for the foot bones where no deviation was found.

In Figure 12 a histogram of the relative differences of the mean doses in all organs and for all treatment plans is plotted.

Table 2 shows a summary of the obtained percentage differences for all patients averaged over all treatment plans and organs.

4 Discussion

The objective of this study was to develop an improved method for whole-body dose reconstruction for patients with limited anatomical data which can be used with a commercial TPS and is applicable to all modern photon treatment technologies. A main application is the dose reconstruction for epidemiological studies which are aimed to assess the risk of late-effects after radiotherapy. Besides this, the tool can be used in daily clinical routine to estimate the dose, e.g. to the fetus of pregnant patients or to the gonads to young male patients.

A major aim of this study was to determine the impact of the whole-body representation on the precision of the whole-body dose calculation. In general, it would be desirable if the whole-body representation would result in uncertainties smaller or equal to the precision of the dose calculation algorithm itself. We compared organ doses between whole-body patient CTs and virtual phantoms which were matched to the treated volume of the patient. The whole-body CTs were chosen such that they cover a wide range of patient ages (from baby to adult). The tumor locations covered a wide spatial range from head to lower abdomen. Finally, a variety of treatment techniques were tested including 3D-CRT, IMRT and VMAT, applied in coplanar and non-coplanar settings and using different nominal beam energies. From these extensive comparisons we found that mean relative differences between organ doses in the different phantoms were ranging between −10% and + 20% with standard deviations of up to 40% (see Table 1). It is interesting to note that the precision of the
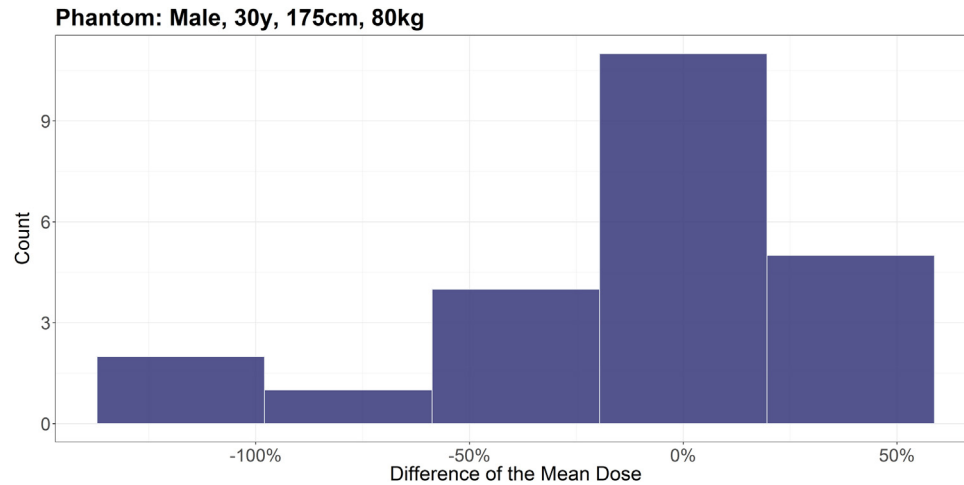
Phantom: Male, 30y, 175cm, 80kg

Figure 12. Out-of-field dose differences between the original whole-body dose representation and the phantom in all organs where the $D_{2\%}$ is less or equal to 5% of the prescribed dose in the two plans for the 38-year-old man with seminoma. In these plans the mean difference of the mean dose per organ -3.1 mGy with a standard deviation of 29.0 mGy. The histogram has a bin width of 0.39.

Table 2
The percentage differences between the mean organ doses on the original CT and on the NCI phantom (averaged over all treatment plans and organs).

Patient	Phantom age/years	Phantom height/cm	Phantom weight/kg	Mean relative difference/%	Standard deviation/%
Baby, female with gluteal rhabdomyosarcoma	0	65	5	−11.9	18.1
Child, female with osteosarcoma of the midear	5	115	15	−0.44	27.9
Adult, female with a breast tumor	30	165	60	2.7	26.7
Adult, male with Hodgkin lymphoma	30	175	65	21.2	31.6
Adult, male with seminoma	30	175	80	−10.2	43

predictions decreases with increasing patient size. However, in some organs the maximum deviations can be as large as 100%. It should be kept in mind, however, that the uncertainty of the dose algorithm itself, obtained by a comparison with measurements, is 11% with a maximum difference below 44%. Thus, the precision of predicting organ doses by matching a real patient to a phantom is approximately of the same order as the precision of the dose calculation.

An advantage of the presented software is its modularity. The different contributions of the out-of-field dose, as it is phantom scatter, collimator scatter, leakage dose and neutron dose can be computed separately [6,14]. As the software is using the API interface of the Varian Eclipse TPS, all tools of a professional planning software can be used to analyze the whole-body dose distribution. In addition, the whole-body dose distributions are stored and archived together with the dose distribution on the limited planning CT.

In its current form, the whole-body representation presented here is based on various simplifications, the most conspicuous of which being the use of a matching algorithm involving simple rigid transformations. A future improvement could be the inclusion of deformable registration. However, it should be noted that deformable registration has the potential to improve matching close to original limited CT, but would likely not improve the dose predictions for organs far from the treated target.

A limitation of the calculation framework developed in the present study is the use of only two electron density values, one for air and lung tissue and one for the remainder organs and tissues. It was shown previously that the resulting calculated dose distributions show satisfying agreement with out-of-field dosimetry [14]. It should be noted that the geometrical uncertainties of the organs of interest make a greater contribution to the final dose error compared to the dose algorithm. The geometrical uncertainty is an unavoidable consequence of using limited patient CT. Hauri et al. [6] showed that the most dominant change in out-of-field dose is along the inferior-superior patient axis. The height of a patient is therefore, the most important parameter for choosing a phantom representation. The effect of geometrical uncertainties for out-of-field dose estimations needs further investigation.

It is planned to commission the algorithms for other treatment machines (such as the Clinac iX and Electa machines). For this, simple ionization chamber measurements are necessary [6].

The presented software is including already a template for the future inclusion of second cancer models which, after the whole-body dose is calculated, allows a real-time estimate of organ specific and whole-body cancer risk.

5 Conclusion

A software package was developed in order to extend the limited patient-CT-information of radiotherapy patients. A whole-body patient representation was achieved by combining the existing CT information with appropriate segmented computational phantoms. The method was confirmed by calculating out-of-field dose distributions on the computational phantoms and comparing them with dose calculations on whole-body patient CTs. The developed method will be useful for epidemiologists and researchers to more accurately estimate organ doses outside the treated volume when only limited treatment planning CT information is available.

Conflict of interest

The authors declare no conflict of interest.

Acknowledgements

Appendix A Supplementary data

Supplementary data associated with this article can be found, in the online version, at https://doi.org/10.1016/j.zemedi.2021.05.001.

References

[1] Miller KD, Siegel RL, Lin CC, Mariotto AB, Kramer JL, Rowland JH, et al. Cancer treatment and survivorship statistics, 2016. CA Cancer J Clin 2016;66:271–89.

[2] Parry C, Kent EE, Mariotto AB, Alfano CM, Rowland JH. Cancer survivors: a booming population. Cancer Epidemiol Biomark Prev 2011;20:1996–2005.

[3] Bhatia S, Sklar C. Second cancers in survivors of childhood cancer. Nat Rev Cancer 2002;2:124–32.

[4] Purdy JA. Dose to normal tissues outside the radiation therapy patient's treated volume: a review of different radiation therapy techniques. Health Phys 2008;95:666–76.

[5] Followill D, Geis P, Boyer A. Estimates of whole-body dose equivalent produced by beam intensity modulated conformal therapy. Int J Radiat Oncol Biol Phys 1997:667–72, http://dx.doi.org/10.1016/s0360-3016(97)00012-6.

[6] Hall EJ, Wuu C-S. Radiation-induced second cancers: the impact of 3D-CRT and IMRT. Int J Radiat Oncol Biol Phys 2003:83–8, http://dx.doi.org/10.1016/s0360-3016(03)00073-7.

[7] Hauri P, Hälg RA, Besserer J, Schneider U. A general model for stray dose calculation of static and intensity-modulated photon radiation. Med Phys 2016:1955–68, http://dx.doi.org/10.1118/1.4944421.

[8] Schneider CW, Newhauser WD, Wilson LJ, Schneider U, Kaderka R, Miljanić S, et al. A descriptive and broadly applicable model of therapeutic and stray absorbed dose from 6 to 25 MV photon beams. Med Phys 2017:3805–14, http://dx.doi.org/10.1002/mp.12286.

[9] Newhauser WD, Schneider C, Wilson L, Shrestha S, Donahue W. A review of analytical models of stray radiation exposures from photon- and proton-beam radiotherapies. Radiat Prot Dosim 2018:245–51, http://dx.doi.org/10.1093/rpd/ncx245.

[10] Mille MM, Jung JW, Lee C, Kuzmin GA, Lee C. Comparison of normal tissue dose calculation methods for epidemiological studies of radiotherapy patients. J Radiol Prot 2018;38:775–92.

[11] Diallo I, Haddy N, Adjadj E, Samand A, Quiniou E, Chavaudra J, et al. Frequency distribution of second solid cancer locations in relation to the irradiated volume among 115 patients treated for childhood cancer. Int J Radiat Oncol Biol Phys 2009:876–83, http://dx.doi.org/10.1016/j.ijrobp.2009.01.040.

[12] Kuzmin GA, Mille MM, Jung JW, Lee C, Pelletier C, Akabani G, et al. A novel method to extend a partial-body CT for the reconstruction of dose to organs beyond the scan range. Radiat Res 2018;189:618–26.

[13] Xu XG. An exponential growth of computational phantom research in radiation protection, imaging, and radiotherapy: a review of the fifty-year history. Phys Med Biol 2014;59(18):R233–302, http://dx.doi.org/10.1088/0031-9155/59/18/R233.

[14] Cristy M. Mathematical phantoms representing children of variousages for use in estimates of internal dose. Oak Ridge, TN: OakRidge National Laboratory; 1980. http://bit.ly/2GckySV.

[15] Geyer AM, O'Reilly S, Lee C, Long DJ, Bolch WE. The UF/NCI family of hybrid computational phantoms representing the current US population of male and female children, adolescents, and adults—application to CT dosimetry. Phys Med Biol 2014:5225–42, http://dx.doi.org/10.1088/0031-9155/59/18/5225.

[16] Kry SF, Bednarz B, Howell RM, Dauer L, Followill D, Klein E, et al. AAPM TG 158 measurement and calculation of doses outside the treated volume from external-beam radiation therapy. Med Phys 2017;44:e391–429.

[17] Lee C, Lodwick D, Hurtado J, Pafundi D, Williams JL, Bolch WE. The UF family of reference hybrid phantoms for computational radiation dosimetry. Phys Med Biol 2010;55:339–63.

[18] Valentin J. Basic anatomical and physiological data for use in radiological protection: reference values. Ann ICRP 2002:1–277, http://dx.doi.org/10.1016/s0146-6453(03)00002-2.

[19] Human alimentary tract model for radiological protection. Ann ICRP 2006;36, i–i.

[20] White DR, Griffith RV, Wilson IJ. Report 46. J ICRU 1992, os24.

[21] Griffin KT, Mille MM, Pelletier C, Gopalakrishnan M, Jung JW, Lee C, et al. Conversion of computational human phantoms into DICOM-RT for normal tissue dose assessment in radiotherapy patients. Phys Med Biol 2019;64, 13NT02.

[22] Hauri P, Schneider U. Whole-body dose equivalent including neutrons is similar for 6 MV and 15 MV IMRT, VMAT, and 3D conformal radiotherapy. J Appl Clin Med Phys 2019;20:56–70.

[23] München HZ. Virtual Human Database. Available from: https://www.helmholtz-muenchen.de/irt/service/virtual-human-download-portal/virtual-human-database/index.html.